

MOA-2012-BLG-505Lb: A super-Earth mass planet in the Galactic bulge

M. Nagakane¹, T. Sumi¹, N. Koshimoto¹, D. P. Bennett^{2,3}, I. A. Bond⁴, N. Rattenbury⁵, D. Suzuki²

and

F. Abe⁶, Y. Asakura⁶, R. Barry², A. Bhattacharya^{2,3}, M. Donachie⁵, A. Fukui⁷, Y. Hirao¹, Y. Itow⁶, M. C. A. Li⁵, C. H. Ling⁴, K. Masuda⁶, Y. Matsubara⁶, T. Matsuo¹, Y. Muraki⁶, K. Ohnishi⁹, C. Ranc², To. Saito¹⁰, A. Sharan⁵, H. Shibai¹, D. J. Sullivan¹¹, P. J. Tristram¹², T. Yamada¹, A. Yonehara¹³
(MOA Collaboration)

ABSTRACT

We report the discovery of a super-Earth mass planet in the microlensing event MOA-2012-BLG-505. This event has the second shortest event timescale

¹Department of Earth and Space Science, Graduate School of Science, Osaka University, 1-1 Machikaneyama, Toyonaka, Osaka 560-0043, Japan

²Laboratory for Exoplanets and Stellar Astrophysics, NASA/Goddard Space Flight Center, Greenbelt, MD 20771, USA

³Department of Physics, University of Notre Dame, Notre Dame, IN 46556, USA

⁴Institute of Information and Mathematical Sciences, Massey University, Private Bag 102-904, North Shore Mail Centre, Auckland, New Zealand

⁵Department of Physics, University of Auckland, Private Bag 92019, Auckland, New Zealand

⁶Institute for Space-Earth Environmental Research, Nagoya University, Nagoya, 464-8601, Japan

⁷Okayama Astrophysical Observatory, National Astronomical Observatory, 3037-5 Honjo, Kamogata, Asakuchi, Okayama 719-0232, Japan

⁸European Southern Observatory (ESO), Karl-Schwarzschildst. 2, D-85748 Garching, Germany

⁹Nagano National College of Technology, Nagano 381-8550, Japan

¹⁰Tokyo Metropolitan College of Industrial Technology, Tokyo 116-8523, Japan

¹¹School of Chemical and Physical Sciences, Victoria University, Wellington, New Zealand

¹²University of Canterbury Mt. John Observatory, P.O. Box 56, Lake Tekapo 8770, New Zealand

¹³Department of Physics, Faculty of Science, Kyoto Sangyo University, Kyoto 603-8555, Japan

of $t_E = 10 \pm 1$ days where the observed data show evidence of planetary companion. Our 15 minute high cadence survey observation schedule revealed the short subtle planetary signature. The system shows the well known close/wide degeneracy. The planet/host-star mass ratio is $q = 2.1 \times 10^{-4}$ and the projected separation normalized by the Einstein radius is $s = 1.1$ or 0.9 for the wide and close solutions, respectively. We estimate the physical parameters of the system by using a Bayesian analysis and find that the lens consists of a super-Earth with a mass of $6.7_{-3.6}^{+10.7} M_\oplus$ orbiting around a brown-dwarf or late M-dwarf host with a mass of $0.10_{-0.05}^{+0.16} M_\odot$ with a projected star-planet separation of $0.9_{-0.2}^{+0.3}$ AU. The system is at a distance of 7.2 ± 1.1 kpc, i.e., it is likely to be in the Galactic bulge. The small angular Einstein radius ($\theta_E = 0.12 \pm 0.02$ mas) and short event timescale are typical for a low-mass lens in the Galactic bulge. Such low-mass planetary systems in the Bulge are rare because the detection efficiency of planets in short microlensing events is relatively low. This discovery may suggest that such low mass planetary systems are abundant in the Bulge and currently on-going high cadence survey programs will detect more such events and may reveal an abundance of such planetary systems.

Subject headings: gravitational lensing: micro

1. Introduction

Since the first discovery of an exoplanet orbiting a main sequence star (Mayor & Queloz 1995), more than 3000 exoplanets have been discovered. Most of these were discovered by the radial velocity method (Butler et al. 2006) and the transit method (Borucki et al. 2011). Although these methods have a higher sensitivity to planets with higher masses and closer orbits in general, their sensitivities are evolving to allow the discovery of planets of lower mass at wider orbits. The Kepler satellite revolutionized our understanding of the exoplanet distribution by detecting many small planets down to Earth-radius planets with semi major axes of less than 1 AU. However the population of low-mass planets with separations of a few AU are less understood.

Exoplanet searches using gravitational microlensing were first proposed by Mao & Paczyński (1991). If a background source star is closely aligned with a foreground lens star, the gravity of the lens bends the light from the source star to create unresolvable images of the source, yielding an apparent magnification of the source star brightness. If the lens star has a planetary companion and it lies close to one of the source images, the gravity of the planet perturbs the observed light curve. Microlensing is uniquely sensitive to exoplanets at orbit radii 1-6 AU, just outside of the snow-line (Ida & Lin 2004; Laughlin et al. 2004; Kennedy et al. 2006) with masses down to Earth mass planets. Contrary to the other planet detection methods mentioned above, microlensing does not rely on any light from the host star. Microlensing is also sensitive to low-mass planets (Bennett & Rhie 1996) orbiting the faint and/or distant stars, like late M-dwarfs, the most common stars in our Galaxy.

Since the first discovery of exoplanets by microlensing (Bond et al. 2004), about 50 planetary microlensing events have been found. Many microlensing planets have been discovered in high-magnification ($A \gtrsim 100$) events. Although the high magnification events are rare, the events are very sensitive to planets (Griest & Safizadeh 1998; Rhie et al. 2000; Rattenbury et al. 2002). Therefore, we issue alerts for high magnification events to encourage follow-up observations to detect and characterize planetary anomalies in the light curves. We report the discovery of a planetary system in the Galactic bulge in the high amplification microlensing event MOA-2012-BLG-505.

We describe the observations and the data set of this event in Section 2. The light curve modeling is described in Section 3. Section 4 presents the data calibration and the source star radius estimate. In Section 5, we present a Bayesian analysis which is used to estimate the physical parameters of the lens system. Finally, our discussion and conclusions are given

in Section 6.

2. Observation and Data

The Microlensing Observations in Astrophysics (MOA; Bond et al. 2001; Sumi et al. 2003) collaboration is conducting a microlensing exoplanet search towards the Galactic bulge using the 1.8m MOA-II telescope at Mt. John University Observatory (MJUO) in New Zealand. Thanks to the wide field of view (FOV) of 2.2 deg^2 with $10\text{k} \times 8\text{k}$ pixel mosaic CCD-camera, MOA-cam3 (Sako et al. 2008), we conduct a high cadence survey observations depending on the field. The observations are carried out mainly with a custom broad $R + I$ band filter, called MOA-Red.

On 2012 July 27, UT 17:48, the microlensing event MOA-2012-BLG-505 was detected and alerted by MOA at $(\alpha, \delta)(2000) = (17^{\text{h}}52^{\text{m}}34^{\text{s}}.34, -32^{\circ}02'24''.33)$ corresponding to Galactic coordinates: $(l, b) = (-1.892^{\circ}, -2.881^{\circ})$. This event was alerted at HJD - 2450000 = 6136.24 and, because the event was very short and fast-rising, the alert was issued after peak magnification and when the planetary signal at the peak was already over. Therefore, no follow-up observation was conducted on this event by other groups. Fortunately, this event occurred in one of fields with the highest cadence observation of 15min. Thus we could detect a short subtle planetary signature by MOA data alone. Figure 1 shows the observed light curve.

The MOA data were reduced with MOA's implementation of a Difference Image Analysis (DIA) pipeline (Bond et al. 2001). This method has an advantage for detecting objects whose brightness changed in the stellar crowded fields like those in the Galactic bulge by subtracting good-quality reference images from each of the observed images. It also produces better photometric light curves, avoiding the effect of blending stars compared to traditional PSF photometry. Moreover, our pipeline is designed to be sensitive to those events whose source star is fainter and not resolved in the reference image, but magnified brighter than observational limiting magnitude by the microlensing, as in this event.

It is known that the nominal error bars calculated by the pipeline are misestimated in such stellar crowded fields due to various reasons. We empirically renormalized the errors by using the standard method (Yee et al. 2012) as follows. Note that this renormalization is intended to get proper errors of the parameters in the light curve modeling, and we made

sure that the fitting results does not depend on this renormalization. We renormalized by using the formula,

$$\sigma'_i = k\sqrt{\sigma_i^2 + e_{min}^2} \quad (1)$$

where σ'_i is the i th renormalized error, σ_i is the i th error obtained from DIA, and k and e_{min} are the renormalizing parameter.

At first, we searched the preliminary best fit model by using light curves with original errors. Then we sort the data points by magnification and make a cumulative χ^2 distribution. The e_{min} value is chosen so as to the slope of distribution to be 1. The k value is chosen so as to $\chi^2/dof \simeq 1$. As a result, we obtained $e_{min} = 0$ and $k = 1.351988$ for MOA-Red, $e_{min} = 0$ and $k = 0.932111$ for MOA-V.

3. Light Curve Models

There are five microlensing parameters for a point-source point-lens (PSPL) model: the time of lens-source closest approach t_0 , the Einstein timescale t_E , the minimum impact parameter in units of the Einstein radius u_0 , the source flux f_S and the blend flux f_B . There are three more parameters for a point-source binary (planetary)-lens model: the planet-host mass ratio q , the planet-host separation in units of the Einstein radius s , the angle between the trajectory of the source and the planet-host axis α . Moreover, if the finite size of the source is considered (finite source effect), we need the source size in units of the Einstein radius $\rho \equiv \theta_*/\theta_E$ where θ_* is the angular source radius, θ_E is the angular Einstein radius. If the effect of Earth's orbital motion during the event, called the microlensing parallax effect, is significant, the north and east components of the microlensing parallax vector $\pi_{E,N}$ and $\pi_{E,E}$ are added, respectively. If both the finite source effect and the microlensing parallax effect are detected, we can determine the lens mass and the distance directly (Muraki et al. 2011).

To fit the microlensing parameters, we used the Markov Chain Monte Carlo (MCMC) algorithm (Verde et al. 2003) and the Sumi et al. (2010) implementation of the image centered ray-shooting method (Bennett & Rhie 1996; Bennett 2010). Three microlensing parameters, (q, s, α) , feature the anomaly shape well, thus we first conduct a grid search of 9680 fixed grid points of these parameters leaving the other parameters free. Then we searched for the best model by refining the best 100 models from the initial grid search with all parameters free. In this event, we detected a finite source effect. To obtain the value of ρ properly,

we included linear limb-darkening. The stellar effective temperature T_{eff} computed from the source color presented in Section 4 is $T_{\text{eff}} \sim 6213$ K (González Hernández & Bonifacio 2009). Assuming $T_{\text{eff}} \sim 6250$ K, surface gravity $\log g = 4.5 \text{ cm s}^{-2}$, microturbulent velocity $v_t = 0 \text{ km s}^{-1}$, and metallicity $\log[M/H] = 0$, we found the limb-darkening coefficient for MOA-Red is $u = 0.52845$ by taking the mean of the R and I-band values. We also determined the coefficient for MOA-V is $u = 0.6413$.

Because the peak magnification of the event is $A_{\text{max}} \sim 100$, the event is very sensitive to the planetary perturbations. Figure 1 shows the best-fit model and the light curve of this event. Table 1 presents the best-fit model parameters. We found that the best-fit model with planetary mass ratio of $q = 2 \times 10^{-4}$ reproduces the asymmetric feature at the peak of light curve in this event. Comparing to the single lens model, the best planetary model improves χ^2 by $\Delta\chi^2 \sim 227$. Therefore, the planetary signal is detected significantly.

The inclusion of the finite source effect improves the fit by $\Delta\chi^2 = 17.1$, i.e., larger than 4σ . The comparison between the model with and without the finite source is shown in Figure 2. One can see that the model with the finite source fits the data better around the event peak. Thus, we include the finite source effect in the following analysis. Because the source trajectory of the best-fit model crosses only the central caustic as is common in high magnification events, there is the well known close-wide degeneracy. The microlensing parameters are almost same except for the separations. The models with $s < 1$ and $s > 1$ are called the close and wide models, respectively. In this event, the shapes of the central caustics for each close and wide models are fairly similar as shown in Figure 3. The χ^2 difference between these models is only $\Delta\chi^2 = 0.019$, therefore we cannot distinguish them.

We did not detect any the microlensing parallax effect in this event. This is as expected because the event is short with timescale of ~ 10 days.

Although the best planetary models have significant $\Delta\chi^2$ compared to the best single lens model, the distinction of these models against stellar binary models is marginal because of relatively subtle anomaly features. In Figure 4, we plot $\Delta\chi^2$ of the models with a range mass ratio q fixed at each grid, and found the local minimums at the stellar mass ratio of $q \sim 6.63 \times 10^{-2}$. $\Delta\chi^2$ of the local minimum with respect to the best model is ~ 31 (i.e., larger than 5σ). Therefore, we conclude that the planetary solution is the global best solution for this event.

Because we were unable to detect microlensing parallax in this event, we cannot determine the physical parameters of the lens system uniquely. Only the measurement of the finite source effect in this event partially breaks the degeneracy between microlensing parameters and that can be used to estimate the probability distribution of the physical parameters via the Bayesian analysis in Section 5.

4. CMD and Source Radius

In this section we estimate the angular Einstein radius $\theta_E = \theta_*/\rho$ from the best fit ρ and the angular source radius θ_* which can be calculated from the source color and magnitude. We get the source color and magnitude from MOA-Red band and MOA-V band data. Figure 5 shows the OGLE (the Optical Gravitational Lensing Experiment; Udalski 2003) $(V - I, I)$ color-magnitude diagram (CMD) of stars within $2'$ around MOA-2012-BLG-505 (Szymański et al. 2011). It also shows the deep CMD of Baade’s window as observed by HST (Holtzman et al. 1998) and which is adjusted for the distance, reddening and extinction to the MOA-2012-BLG-505 field by using Red Clump Giants (RCG) as standard candles (Bennett et al. 2008). We convert the best fit MOA-Red and MOA-V source magnitude to the standard Cousins I and Johnson V magnitude by cross-referencing stars in the MOA field with stars in the OGLE-III photometry map (Szymański et al. 2011) within $2'$ of the event. We find the source color and magnitude to be $(V - I, I)_{S,OGLE} = (2.00, 21.29) \pm (0.06, 0.13)$. We only have a couple of MOA-V data points, one highly magnified point and one with low magnification, during this event. So we doubled the nominal error of the source color conservatively. We find, therefore, the source color and magnitude to be $(V - I, I)_{S,OGLE} = (2.00, 21.29) \pm (0.12, 0.13)$. The centroid of RCG color and magnitude in CMD are $(V - I, I)_{RCG} = (2.49, 16.32) \pm (0.01, 0.03)$ as shown in Figure 5. Comparing these values to the expected extinction-free RCG color and magnitude at this field of $(V - I, I)_{RCG,0} = (1.06, 14.55) \pm (0.07, 0.04)$ (Bensby et al. 2013; Nataf et al. 2013), we get the reddening and extinction to the source of $(E(V - I), A_I)_{RCG} = (1.43, 1.77) \pm (0.07, 0.05)$. Therefore, we estimated the extinction-free source color and magnitude as being

$$(V - I, I)_{S,0} = (0.57, 19.52) \pm (0.14, 0.14). \quad (2)$$

By using the empirical formula, $\log(\theta_*) = 0.50141358 + 0.41968496(V - I) - 0.2I$ (Boyajian et al. 2014; Fukui et al. 2015), we estimated the angular source radius,

$$\theta_* = 0.34 \pm 0.05 \mu\text{as}. \quad (3)$$

From this θ_* and other fitting parameters, we calculated the angular Einstein radius θ_E and the lens-source relative proper motion $\mu_{\text{rel}} = \theta_E/t_E$, as follows,

$$\theta_E = 0.12 \pm 0.02 \text{ mas} \quad (4)$$

$$\mu_{\text{rel}} = 4.40 \pm 0.72 \text{ mas yr}^{-1} \quad (5)$$

This θ_E is relatively small which indicates that lens is likely low-mass and/or far from the observer. This μ_{rel} is relatively high which prefers that the lens is in the Galactic bulge rather than the disk.

The source color obtained from MOA-Red and MOA-V data lies on the blue edge of the typical main sequence stars expected from the HST CMD. We checked the effect of possible systematics in the color measurement on the final estimated lens physical parameters as follows. Assuming the source star is a main sequence star in the Bulge, which is very likely, we adopt the mean color of the main sequence stars in the HST CMD with the magnitudes ranging around the observed source magnitude $I_S = 21.29 \pm 0.13$ (Bennett et al. 2008). We get a source color and magnitude of $(V - I, I)_{\text{S,OGLE}} = (2.32, 21.29) \pm (0.12, 0.13)$ and $(V - I, I)_{\text{S,0}} = (0.89, 19.52) \pm (0.14, 0.14)$, with and without extinction and reddening, respectively.

The lens physical parameters estimated by using this source color are consistent with the final results by using the source color obtained from the light curves (see Section 5) to within 1σ errors. Therefore, systematics in our measurement of the source color do not make any difference to our final results. We use the source color measured from the light curves in the following discussions.

5. Lens Physical Parameters by Bayesian Analysis

We can not directly determine the lens physical parameters because we couldn't measure the microlensing parallax effect. Thus we estimated the probability distribution of lens physical properties by using a Bayesian analysis (Beaulieu et al. 2006; Gould et al. 2006; Bennett et al. 2008) assuming the Galactic model of Han & Gould (1995) as a prior probability. We note that the probability of stars hosting a planet with the measured q and s values is independent of the lens's mass and distance from the Earth. We used the measured θ_E and t_E to constrain the probability distributions of lens parameters. Although this event has the $s \leftrightarrow 1/s$ degeneracy, all lens physical parameters of these degenerate solutions are consistent within the 68.3% confidence interval. Therefore, we combined the result of wide and close model weighted by $e^{-\Delta\chi^2/2}$ ($\Delta\chi^2 = \chi_{\text{close}}^2 - \chi_{\text{wide}}^2 = 0.019$).

The distributions and parameters are shown in Figure 6, Figure 7 and Table 2, respectively. According to this analysis, the host is a brown-dwarf or late M-dwarf with a mass of $0.10_{-0.05}^{+0.16}M_{\odot}$ at $7.21_{-1.11}^{+1.14}$ kpc away from the Earth i.e., likely in the Galactic bulge. The planet mass is a super-Earth with a mass of $6.7_{-3.6}^{+10.7}M_{\oplus}$ and the projected separation from the host is $r_{\perp} = 0.91_{-0.23}^{+0.26}$ AU. Assuming a planetary orbit with random inclination and phase (Gould & Loeb 1992), the physical three-dimensional separation is $a = 1.13_{-0.34}^{+0.68}$ AU.

6. Discussion and Conclusion

We found that MOA-2012-BLG-505Lb is a super-Earth mass planet, ranging from terrestrial mass to Neptune mass, orbiting around a brown-dwarf or late M-dwarf in the Galactic bulge. Figure 8 shows the distribution of known exoplanets in planet mass as a function of the host mass. This event is shown by a purple circle and the position is bottom-left (corresponding to both a low-mass host and planet). The red circles indicate the planets found by microlensing, where filled and open circles indicates that their masses are measured and estimated by a Bayesian analysis, respectively. Red ones indicate planetary mass ratios of $q \leq 0.1$ and green ones, on the other hand, indicate larger mass ratios of $q > 0.1$, i.e., low mass binaries. Although the detection efficiencies of the planetary events with large q are higher than that with small q (Suzuki et al. 2016), all of planetary systems have small $q \sim 0.001 - 0.0001$ except one planetary system with large $q \sim 0.01$ (Han et al. 2016) orbiting around low-mass stars of $< 0.15M_{\odot}$. This result indicates that the low-mass stars tend to host relatively low-mass planetary companions.

This event has the second shortest t_E with a planetary companion after MOA-2011-BLG-262 (Bennett et al. 2014). Only a few microlensing planets with $t_E \lesssim 10$ days have been found. This is largely because the detection efficiency of planets in short events is low (Suzuki et al. 2016). We need to find and analyze more events like MOA-2012-BLG-505, to obtain unbiased statistics of planets around low-mass hosts.

Penny et al. (2016) indicates that the massive samples of exoplanets should be possible to probe the distribution of various exoplanet populations as a function of their host’s location within the Galaxy. There are five planets which locate $D_L > 6.0$ kpc with 1σ lower limit, i.e., likely in the Bulge, MOA-2011-BLG-028Lb (Skowron et al. 2016), MOA-2008-BLG-310Lb (Janczak et al. 2010), OGLE-2015-BLG-0051Lb (Han et al. 2016), MOA-2011-BLG-293Lb (Batista et al. 2014) and MOA-2011-BLG-322Lb (Shvartzvald et al. 2014). MOA-

2011-BLG-028Lb, MOA-2008-BLG-310Lb and OGLE-2015-BLG-0051Lb are a Neptune-mass planet, Sub-Saturn mass planet and a sub-Jupiter mass planet in the Galactic bulge, respectively. MOA-2011-BLG-293Lb and MOA-2011-BLG-322Lb are super-Jupiter mass planets in the Galactic bulge. MOA-2012-BLG-505Lb is the sixth planet which is likely to be in the Bulge. This discovery contributes to the statistics of planet distribution in our Galaxy.

We used the Bayesian analysis to estimate the probability distribution of the lens physical parameters because we couldn't measure the microlensing parallax. It is difficult to observe the microlensing parallax in the Bulge lens events because they are relatively short and their projected Einstein radius on the observer plane, \tilde{r}_E is large relative to 1 AU. \tilde{r}_E for the Bulge lens event is $3 \sim 10$ AU typically. It is difficult to detect the microlensing parallax for such events from the space telescope located at L2, however we may be able to detect these from the telescope located on \sim AU away from the Earth like Spitzer (Street et al. 2016) and/or Kepler (Henderson et al. 2016). If these instruments observe many events similar to MOA-2012-BLG-505, they will be able to determine the planet distribution in the Galaxy down to low-mass hosts. NASA's WFIRST satellite will increase this sample size significantly and reveal the Galactic distribution of exoplanets (Spergel et al. 2015).

We may identify the lens by future high resolution imaging with space telescope or ground base AO observation if it is a relatively massive star, or we may set a tight upper limit when it is really low-mass star. Figure 7 shows the distributions of I , J , H , and K -band magnitudes for the lens star with extinction. The lens magnitudes are estimated from Kenyon & Hartmann (1995) and Baraffe et al. (2003). We selected the isochrone model for a 5 Gyr brown-dwarf from Baraffe et al. (2003). The extinctions are estimated by using Cardelli et al. (1989). The distributions look bimodal because the luminosity changes sharply around $0.07M_\odot$, i.e., at the boundary between brown-dwarf and main sequence stars, in the mass-luminosity relation. We cannot detect the lens star if it is brown-dwarf. However if the lens star is a hydrogen burning star, probably we will be able to detect it with JWST (Gardner et al. 2006) when it is separated from the source star after 10 years.

TS acknowledges the financial support from the JSPS, JSPS23103002, JSPS24253004 and JSPS26247023. The MOA project is supported by the grant JSPS25103508 and 23340064. Work by N.K. is supported by JSPS KAKENHI Grant Number JP15J01676. NJR is a Royal Society of New Zealand Rutherford Discovery Fellow. AS is a University of Auckland Doctoral Scholar.

REFERENCES

- Baraffe, I., Chabrier, G., Barman, T. S., Allard, F., & Hauschildt, P. H. 2003, *A&A*, 402, 701
- Batista, V., Beaulieu, J.-P., Gould, A., et al. 2014, *ApJ*, 780, 54
- Beaulieu, J.-P., Bennett, D. P., Fouqué, P., et al. 2006, *Nature*, 439, 437
- Bennett, D. P. 2010, *ApJ*, 716, 1408
- Bennett, D. P., Batista, V., Bond, I. A., et al. 2014, *ApJ*, 785, 155
- Bennett, D. P., Bond, I. A., Udalski, A., et al. 2008, *ApJ*, 684, 663-683
- Bennett, D. P., & Rhie, S. H. 1996, *ApJ*, 472, 660
- Bensby, T., Yee, J. C., Feltzing, S., et al. 2013, *A&A*, 549, A147
- Bond, I. A., Abe, F., Dodd, R. J., et al. 2001, *MNRAS*, 327, 868
- Bond, I. A., Udalski, A., Jaroszyński, M., et al. 2004, *ApJ*, 606, L155
- Borucki, W. J., Koch, D. G., Basri, G., et al. 2011, *ApJ*, 736, 19
- Boyajian, T. S., van Belle, G., & von Braun, K. 2014, *AJ*, 147, 47
- Butler, R. P., Wright, J. T., Marcy, G. W., et al. 2006, *ApJ*, 646, 505
- Cardelli, J. A., Clayton, G. C., & Mathis, J. S. 1989, *ApJ*, 345, 245
- Fukui, A., Gould, A., Sumi, T., et al. 2015, *ApJ*, 809, 74
- Gardner, J. P., Mather, J. C., Clampin, M., et al. 2006, *Space Sci. Rev.*, 123, 485
- González Hernández, J. I., & Bonifacio, P. 2009, *A&A*, 497, 497
- Gould, A., & Loeb, A. 1992, *ApJ*, 396, 104
- Gould, A., Udalski, A., An, D., et al. 2006, *ApJ*, 644, L37
- Griest, K., & Safizadeh, N. 1998, *ApJ*, 500, 37
- Han, C., & Gould, A. 1995, *ApJ*, 447, 53
- Han, C., Udalski, A., Gould, A., et al. 2016, *AJ*, 152, 95

Henderson, C. B., Poleski, R., Penny, M., et al. 2016, *PASP*, 128, 124401

Henderson, C. B., & Shvartzvald, Y. 2016, *AJ*, 152, 96

Holtzman, J. A., Watson, A. M., Baum, W. A., et al. 1998, *AJ*, 115, 1946

Ida, S., & Lin, D. N. C. 2004, *ApJ*, 616, 567

Janczak, J., Fukui, A., Dong, S., et al. 2010, *ApJ*, 711, 731

Kennedy, G. M., Kenyon, S. J., & Bromley, B. C. 2006, *ApJ*, 650, L139

Kenyon, S. J., & Hartmann, L. 1995, *ApJS*, 101, 117

Laughlin, G., Bodenheimer, P., & Adams, F. C. 2004, *ApJ*, 612, L73

Mao, S., & Paczyński, B. 1991, *ApJ*, 374, L37

Mayor, M., & Queloz, D. 1995, *Nature*, 378, 355

Muraki, Y., Han, C., Bennett, D. P., et al. 2011, *ApJ*, 741, 22

Nataf, D. M., Gould, A., Fouqué, P., et al. 2013, *ApJ*, 769, 88

Penny, M. T., Henderson, C. B., & Clanton, C. 2016, *ApJ*, 830, 150

Rattenbury, N. J., Bond, I. A., Skuljan, J., & Yock, P. C. M. 2002, *MNRAS*, 335, 159

Rhie, S. H., Bennett, D. P., Becker, A. C., et al. 2000, *ApJ*, 533, 378

Sako, T., Sekiguchi, T., Sasaki, M., et al. 2008, *Experimental Astronomy*, 22, 51

Shvartzvald, Y., Maoz, D., Kaspi, S., et al. 2014, *MNRAS*, 439, 604

Skowron, J., Udalski, A., Poleski, R., et al. 2016, *ApJ*, 820, 4

Spergel, D., Gehrels, N., Baltay, C., et al. 2015, *arXiv:1503.03757*

Street, R. A., Udalski, A., Calchi Novati, S., et al. 2016, *ApJ*, 819, 93

Sumi, T., Abe, F., Bond, I. A., et al. 2003, *ApJ*, 591, 204

Sumi, T., Bennett, D. P., Bond, I. A., et al. 2010, *ApJ*, 710, 1641

Suzuki, D., Bennett, D. P., Sumi, T., et al. 2016, *ApJ*, 833, 145

Szymański, M. K., Udalski, A., Soszyński, I., et al. 2011, *Acta Astron.*, 61, 83

Udalski, A. 2003, *Acta Astron.*, 53, 291

Verde, L., Peiris, H. V., Spergel, D. N., et al. 2003, *ApJS*, 148, 195

Yee, J. C., Shvartzvald, Y., Gal-Yam, A., et al. 2012, *ApJ*, 755, 102

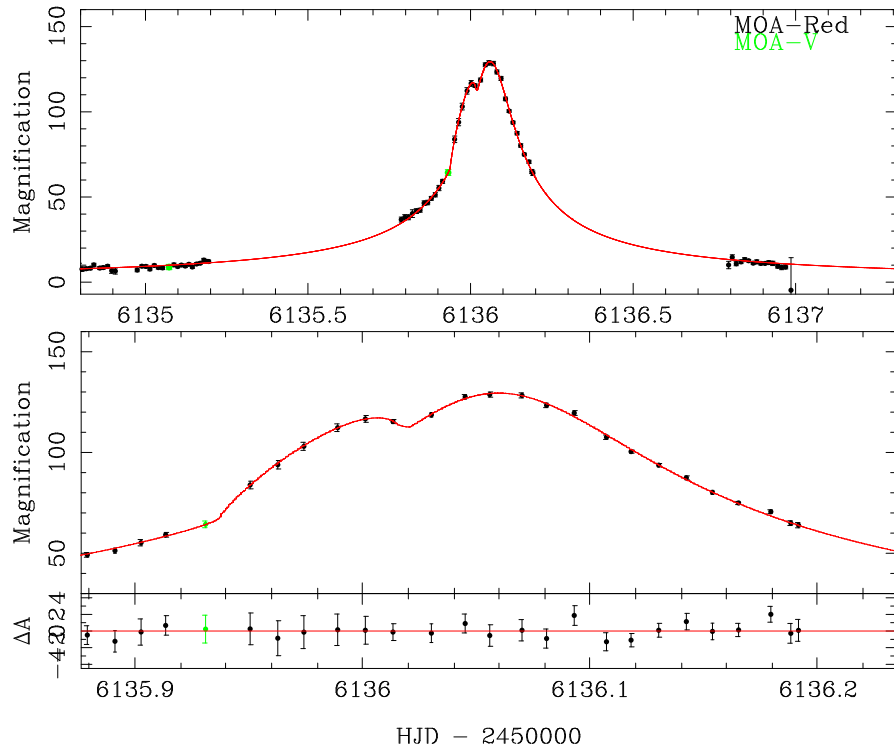


Fig. 1.— The light curve of event MOA-2012-BLG-505 with data from MOA-Red (black) and MOA-V (Green). The best-fit model is indicated by the red line. Middle and bottom panels show the detail of planetary signal and the residual from the best model respectively.

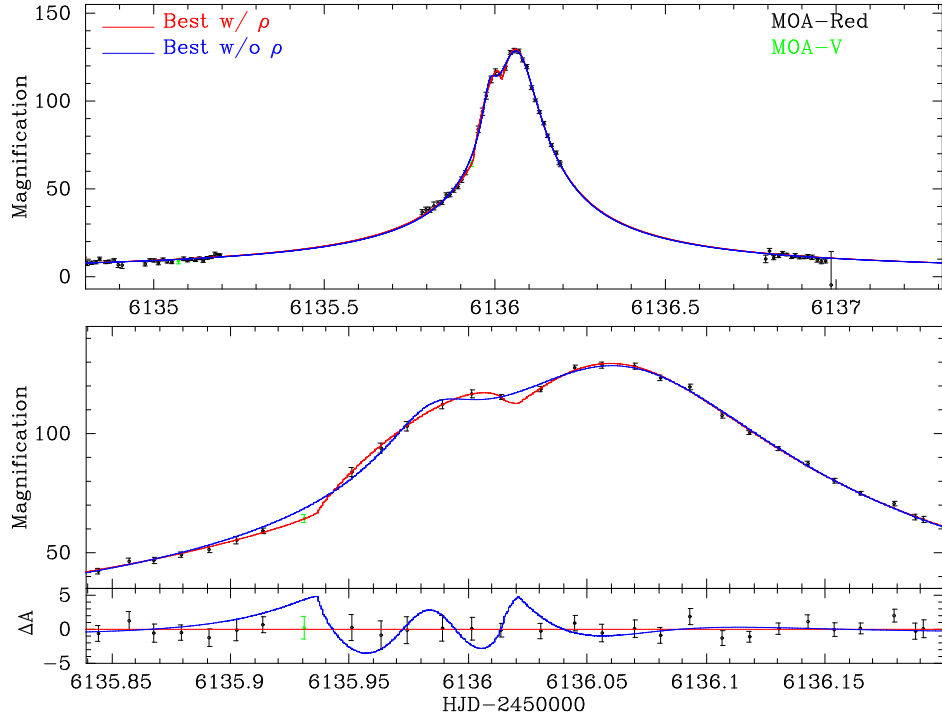


Fig. 2.— The best-fit model fitted with the finite source effect (red line) and the best-model fitted without the finite source effect (blue line). The χ^2 of blue line is $\Delta\chi^2 \sim 17.1$ larger than red one.

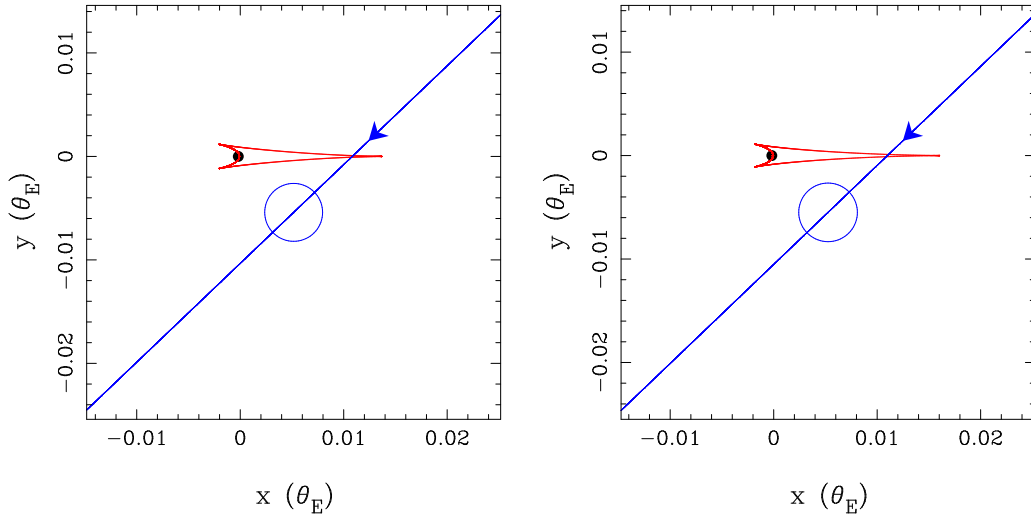


Fig. 3.— Caustic geometries for the best-fit close (left) and wide (right) models indicated by the red curves. The blue line for each figures shows the source trajectory with respect to the lens system. The blue circle for each figures indicates the source star size.

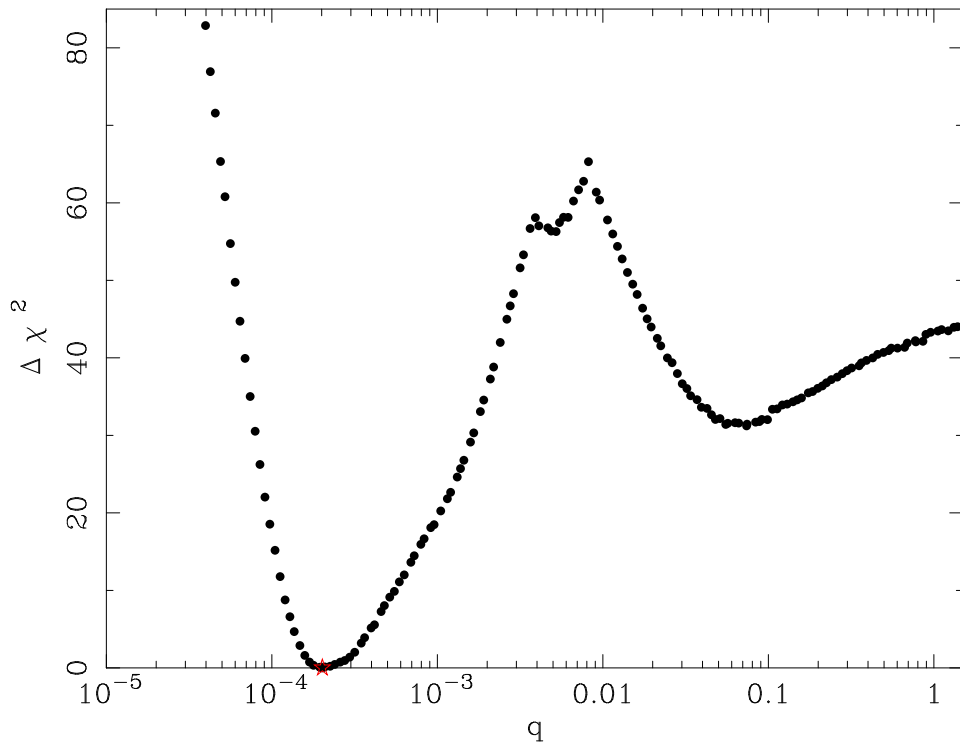


Fig. 4.— $\Delta\chi^2$ from the best-fit model as a function of q . The red star indicates the $\Delta\chi^2$ and q values corresponding to the best fitting model. There is a local minimum at $q \sim 6.63 \times 10^{-2}$, and $\Delta\chi^2$ between the best and local minimum is about 31.

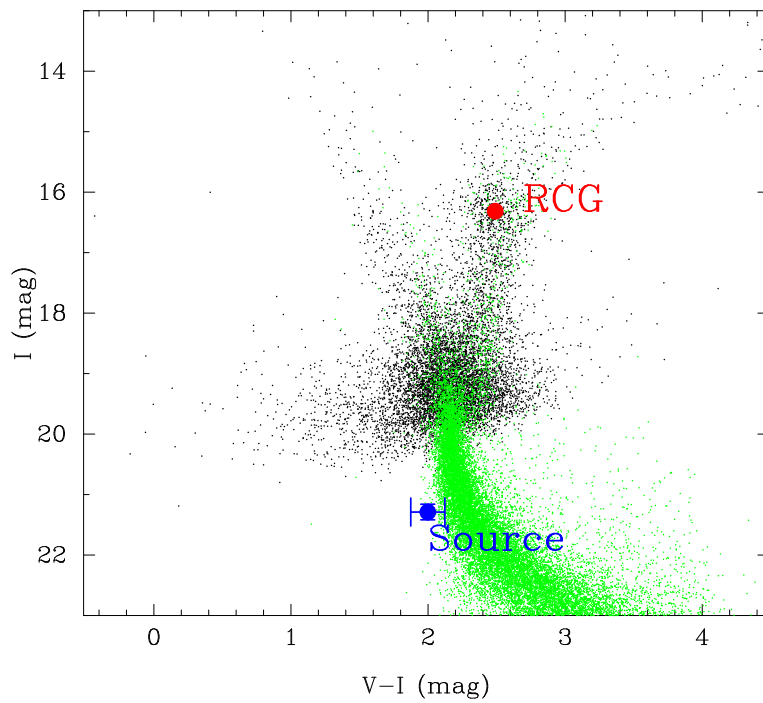


Fig. 5.— Color Magnitude Diagram (CMD) of OGLE-III stars within 2' of MOA-2012-BLG-505 (black dots). The green dots show the HST CMD (Holtzman et al. 1998). The red point indicates the centroid of red clump giant, and the blue point indicates the source color and magnitude.

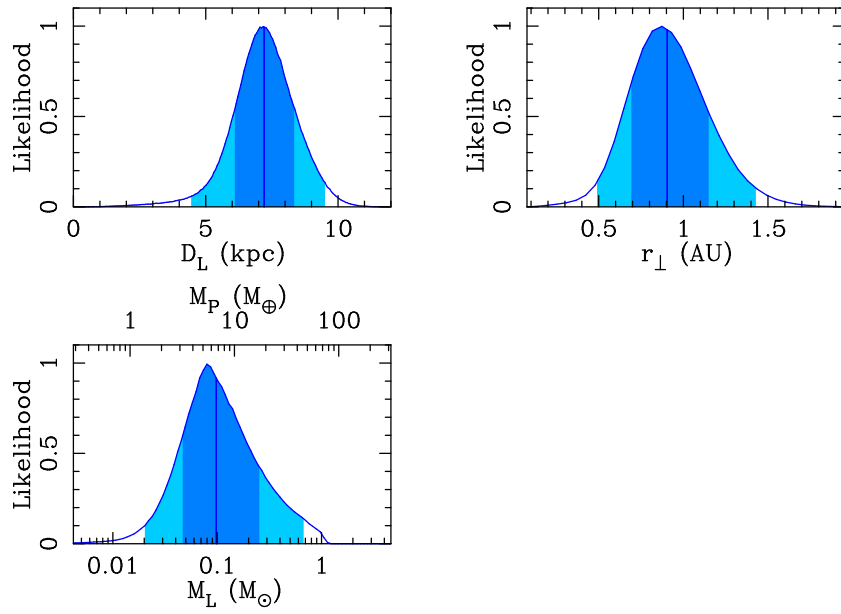


Fig. 6.— Relative probability distributions of lens system properties from our Bayesian analysis. The dark and light blue regions indicate the 68% and 95% confidence intervals respectively. The blue vertical lines indicate the median values of each of these distributions.

Table 1: The best-fit parameters and 1σ errors for close and wide models

parameter	units	close	wide
error (1σ)		($s < 1$)	($s > 1$)
t_0	HJD - 2450000	6136.0557	6136.0558
		0.0005	0.0005
t_E	days	10.0133	9.8335
		1.0035	1.0506
u_0	10^{-3}	7.4775	7.6002
		0.8810	0.8568
q	10^{-4}	2.0520	2.0521
		0.5647	0.5528
s		0.8928	1.1266
		0.0477	0.0653
α	radians	2.3794	2.3782
		0.0175	0.0160
ρ	10^{-3}	2.7971	2.8322
		0.3714	0.3703
θ_*	μas	0.342	0.342
		0.052	0.052
θ_E	mas	0.122	0.121
		0.025	0.024
μ_{rel}	mas yr^{-1}	4.3890	4.3971
		0.7198	0.7196
<i>d.o.f.</i>		16004	16004
χ^2		16010.859	16010.840

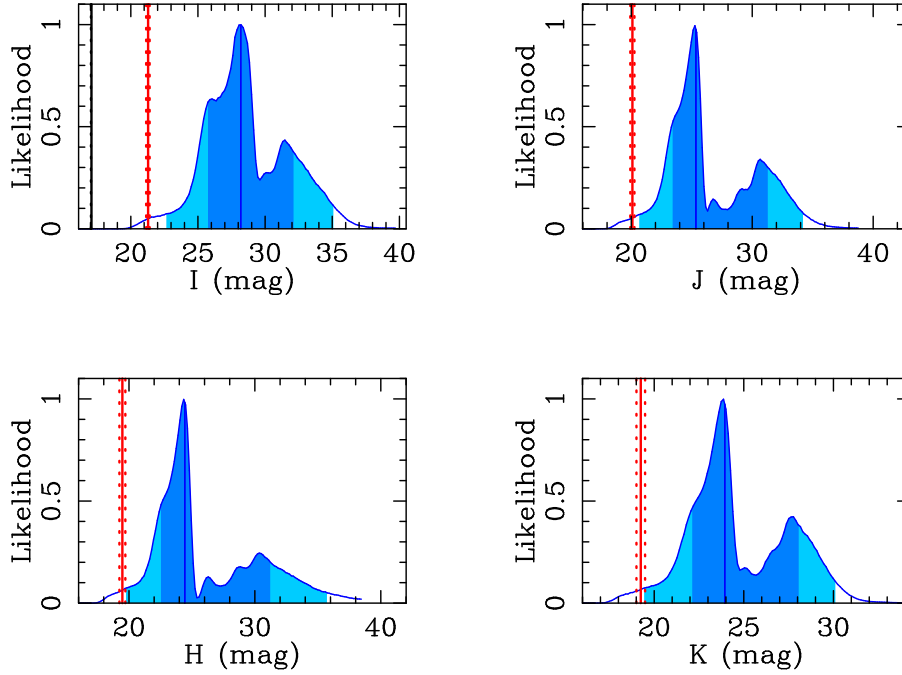


Fig. 7.— Relative probability distributions for the I , J , H and K -band lens star magnitudes from our Bayesian analysis with extinction. The dark and light blue regions indicate the 68% and 95% confidence intervals respectively. The vertical blue lines indicate the median values of each of these distributions. The vertical red lines indicate the source star magnitudes for each bands. Red dotted lines are their 1σ errors. The source magnitudes are estimated from Kenyon & Hartmann (1995) and Baraffe et al. (2003). Their extinctions are estimated from Cardelli et al. (1989).

Table 2: The physical parameters and 1σ errors of MOA-2012-BLG-505

parameter	units	value	error(1σ)
D_L	kpc	7.21	+1.14 -1.11
M_L	M_\odot	0.10	+0.16 -0.05
m_p	M_\oplus	6.70	+10.61 -3.51
r_\perp	AU	0.90	+0.25 -0.21
a	AU	1.12	+0.67 -0.32
μ	mas yr^{-1}	4.72	+1.01 -0.91
J	mag	25.34	+5.94 -1.92
H	mag	24.43	+6.79 -1.89
K	mag	23.93	+4.13 -1.82

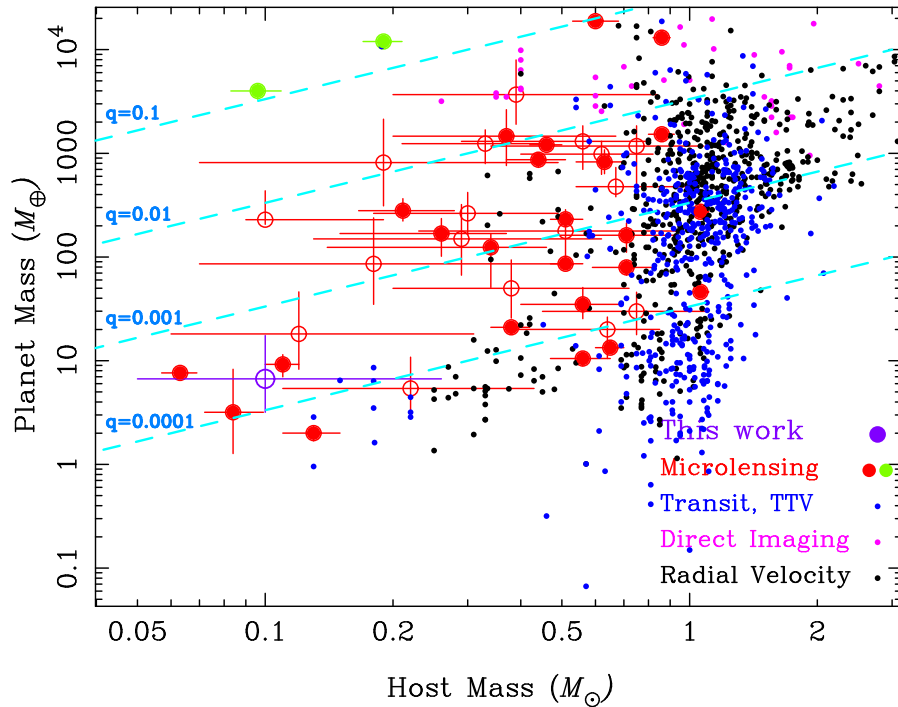


Fig. 8.— Distribution of exoplanets. The horizontal axis corresponds to the host mass and the vertical axis corresponds to the planet mass. The purple point indicates MOA-2012-BLG-505. The red, green, blue, magenta and black points indicate the planets found by Microlensing (planetary mass companion), Microlensing (binary mass companion), Transit & TTV, Direct Imaging, and Radial Velocity, respectively. In Microlensing planets, filled circles indicates that their masses are measured and open circles indicate that their masses are estimated by a Bayesian analysis.